NASA

Technical Memorandum 80596

Tropical Cyclone Rainfall Characteristics as determined from a Satellite Passive Microwave Radiometer

E. B. Rodgers and R. F. Adler

DECEMBER 1979

National Aeronautics and
Space Administration

Goddard Space Flight Center
Greenbelt, Maryland 20771

Tropical Cyclone Rainfall Characteristics As Determined From a Satellite Passive Microwave Radiometer

Edward B. Rodgers and Robert F. Adler
Laboratory for Atmospheric Sciences (GLAS)
Goddard Space Flight Center
National Aeronautics and Space Administration
Greenbelt, MD 20771

ABSTRACT

Data from the Nimbus-5 Electrically Scanning Microwave Radiometer (ESMR-5) have been used to calculate latent heat release (LHR) and other rainfall parameters for over 70 satellite observations of 21 tropical cyclones during 1973, 1974, and 1975 in the tropical North Pacific Ocean. The results indicate that the ESMR-5 measurements can be useful in determining the rainfall characteristics of these storms and appear to be potentially useful in monitoring as well as predicting their intensity. The ESMR-5 derived total tropical cyclone rainfall estimates agree favorably with previous estimates for both the disturbance and typhoon stages. The mean typhoon rainfall rate (1.9 mm h^{-1}) is approximately twice that of disturbances (1.1 mm h^{-1}).

Case studies suggest that tropical cyclone intensification is indicated by the increase in the ESMR-5 derived LHR, the increase in the relative contribution of the heavier rain rates ($\geqslant$5 mm h^{-1}) to the total storm rainfall, and the decrease in the radius of maximum rain rate from the cyclone center. It also appears evident from these case studies that by monitoring the trend of increasing LHR the first indication of tropical cyclone intensification may be obtained 1-2 days prior to the tropical cyclone reaching storm stage and often prior to the first reconnaissance aircraft observation. Further, the time of the maximum intensity of the tropical cyclone lags by 1-2 days the time of maximum LHR. The statistics of the Western Pacific tropical cyclones confirm the case study results in that tropical cyclone intensity can be monitored from ESMR-5 derived rainfall parameters. As the mean tropical cyclone intensifies from a disturbance to typhoon stage the average LHR increases steadily. The mean relative contribution of the heavier rain rate ($\geqslant$5 mnh^{-1}) to the total storm rainfall increased from .24 at depression stage to .33 at storm stage and finally to .39 at typhoon stage. The radial distance of the maximum rain rate from the center decreases with intensification while the azimuthal distribution indicates a slight preference for maximum rain rate in the right half of the composite storm at all stages. The study also indicates that Eastern Pacific hurricanes have less LHR, are more compact, and have less intense rainfall than the Western Pacific typhoons.

CONTENTS

TABLES

1. INTRODUCTION

The maintenance of mature tropical cyclones is dependent on the release of latent heat. The heat generated by the condensation process and by the adiabatic warming associated with descending motion within the center of circulation produces the central positive temperature anomaly in hurricanes and typhoons. This generated heat will then hydrostatically lower the pressure within the column below the tropopause and thereby creating the pressure gradient necessary to intensify the storm's circulation. A number of studies (e.g., Palmen and Riehl, 1957) indicate that the outflow of energy is nearly equal to the storm's latent heat release (LHR), for steady state conditions.

The role of LHR in tropical cyclogenesis and storm intensification is less obvious. Statistical analysis of pibal and rawinsonde wind data over the tropical oceans by Ahr (1976) and Erickson (1977) showed that the average divergence patterns, and therefore, mean vertical motion and rainfall within 444 and 666 km radius of the center of circulation of developing Western Pacific disturbances are approximately the same as that for non-developing systems. Furthermore, Arnold (1977) and Erickson (1977) demonstrated from the Defense Military Satellite Program (DMSP) satellite data that developing systems often have similar amounts of deep penetrative convection and/or area of cirrus shield than non-developing systems. Thus, tropical cyclogenesis does not appear to be related solely to the magnitude of cumulus convection and vertical motion, and therefore, LHR. However, it is postulated that the intensification of tropical systems from depression to storm and hurricane stage is closely related to increasing low level convergence, high level divergence, and therefore, vertical motion and LHR through the mechanism of Conditional Instability of the Second Kind (CISK) (Ooyama, 1964; Charney and Eliassen, 1964). Studying the time evolution of tropical cyclone rainfall should help establish whether the mass or the motion field intensifies first in the cyclogenesis and intensification phases of hurricane and typhoon development. This, in turn, may lead to methods of using satellite data to detect or predict tropical cyclone development.

Previous estimates of the LHR in tropical cyclones have been made using the moisture budget approach in which conventional and aircraft winds together with water vapor measurements were used to calculate the lateral flux of moisture or latent heat across a boundary of a storm (Miller, 1962; Palmen and Riehl, 1957; Riehl and Malkus, 1961). Assuming steady-state the condensation and precipitation inside the boundary are approximately equivalent to the boundary flux. Radar observations of tropical cyclone precipitation has added considerably to the understanding of the storm structure, however, no estimates of storm LHR have been made with radar data.

The estimate of LHR in tropical cyclones by either the moisture budget approach or radar at a frequency necessary to monitor intensity changes would be difficult particularly for storms over the open ocean areas. An alternative method to frequently monitor tropical cyclone LHR over ocean areas is to use satellite-flown, passive microwave radiometer measurements as suggested by Adler and Rodgers (1977). This study revealed that the calculation of LHR from the Nimbus-5 Electrically Scanning Microwave Radiometer (ESMR-5) for a Western Pacific tropical cyclone (Nora, September and October 1973) was comparable with estimates made by other investigators for mature storms and that as the storm intensified the LHR increased, the rainfall concentrated towards the center of circulation, and the relative contribution of the heavier rain rates increased. Since the results from this study suggest that ESMR-5 data can be used to estimate tropical cyclone LHR and possibly monitor intensity changes, there is an incentive to further substantiate this approach with more cases. This paper presents results from the calculation of the magnitude and distribution of rainfall in Pacific Ocean tropical cyclones using the EMSR-5 data. Approximately 70 satellite passes over tropical cyclones in various states of development are used. All storms examined reached typhoon/hurricane stage sometime during their lifetime.

2. DESCRIPTION OF DATA

The Nimbus-5 spacecraft, which was launched in December 1972, has a sun synchronous orbit with local noon and midnight equator crossings at an altitude of approximately 1100km. Successive orbits of the spacecraft cross the equator with a separation of 27° longitude as a result of the earth's rotation during the approximate 107 minute orbital period. The ESMR-5 is a passive microwave instrument that measures horizontally polarized emitted radiation in the 19.35 GHz (1.55 cm) region. The instrument antenna scans perpendicular to the spacecraft forward motion from left to right within 50° of nadir in 78 steps every 4 seconds. This produces an approximate 2500 km ground swath and an orbit to orbit coverage overlap at the equator. However, the useable swath is limited by degradation in the ground resolution. At nadir the instantaneous field of view (IFOV) is nearly a circle approximately 25 km in diameter at the earth surface and degrades to an oval having dimensions of approximately 45 X 160 km at 50° off nadir. In this study, scan points that fell only within 40° of nadir were used (ground resolution at 40° of nadir is approximately 30 X 70 km). A swath ±40° of nadir (approximately 1700km ground swath) does not produce any overlap between adjacent orbits at the equator. Further details of the ESMR-5 are discussed by Wilheit (1972).

The brightness temperature (T_B) measured by the ESMR-5 is a function of radiation emerging from the earth's surface, the intervening atmosphere between the satellite and the earth, and the radiometer viewing angle. The microwave energy emitted from the earth's surface at 19.35 GHz is dependent upon the earth's thermodynamic temperature and its emissivity. The emissivity varies due to the change in the dielectric constant of the emitting surface. For example, land areas without vegetation that contain dry soils with a low dielectric constant have a high emissivity of approximately 0.95, while water surfaces with a high dielectric constant will have a low emissivity of about 0.40. This results in a T_B contrast of approximately 100K difference between land (T_B ~ 215 to 300K) and water (T_B ~ 120 to 170K) in clear areas. Over water the T_B variation is mainly dependent upon ocean surface roughness, and wind driven foam. From NASA Convair 990 flights using a similiar

passive microwave radiometer over ocean surfaces with various sea surface wind speeds, Nordberg, et al. (1971) showed that there is a linear relationship between sea surface wind speed (>7 ms^{-1}) and enhanced T_B. It was found that wind speed of 20 ms^{-1} enhances the T_B at nadir by approximately 7 5K.

Within the intervening atmosphere, the ESMR-5 T_B values are affected by molecular oxygen, atmospheric water vapor, and liquid water. The greatest effect is due to enhanced absorption by liquid water, particularly large droplets and rain with radii greater than 1 mm. The effects of the emission from raindrops is best observed over calm ocean areas since the oceans act as a mirror due to its low uniform emissivity (high uniform reflectivity). Large contrasts can exist between rain enhanced T_B and T_B measurements of the reflected background space energy from off the ocean and the atmospheric molecular oxygen and water vapor. Ice crystal clouds are relatively transparent to microwave energy at this frequency.

An example of the rainfall distribution in a tropical cyclone as observed from ESMR-5 is shown in Fig. 1 which depicts a series of ESMR-5 images and the simultaneous Nimbus 5 Temperature Humidity Infrared Radiometer (THIR) 11.5 μm images of tropical cyclone Irma (Western Pacific Ocean 19-26 November, 1974). The lightest shades on both the IR and ESMR-5 image depicts the coldest T_{BB} and T_B respectively. The darkest shades in the ESMR-5 images depict rain as well as land features (i.e. Philippine Islands on the western edge of 25 November ESMR-5 image in Fig. 1). In the rain areas, the darker the shade (the warmer the T_B) the more intense the rainfall. The EMSR-5 images are shown so that only the T_B values between 194-266 are displayed. The figure demonstrates that there is not a complete match between cloud configuration and rainfall distribution. There is a considerable amount of non-precipitating ice and low stratiform clouds that are not being detected by ESMR-5. The ESMR-5 images also reveal features that are related to tropical cyclone intensification that are not apparent on the THIR images. For example, as Irma intensifies the areal distribution and intensification of the rainfall increases. Also the curvature of these rainbands increased and moved towards the center of circulation. Another feature related to intensification that is best observed in the ESMR-5 images is an early

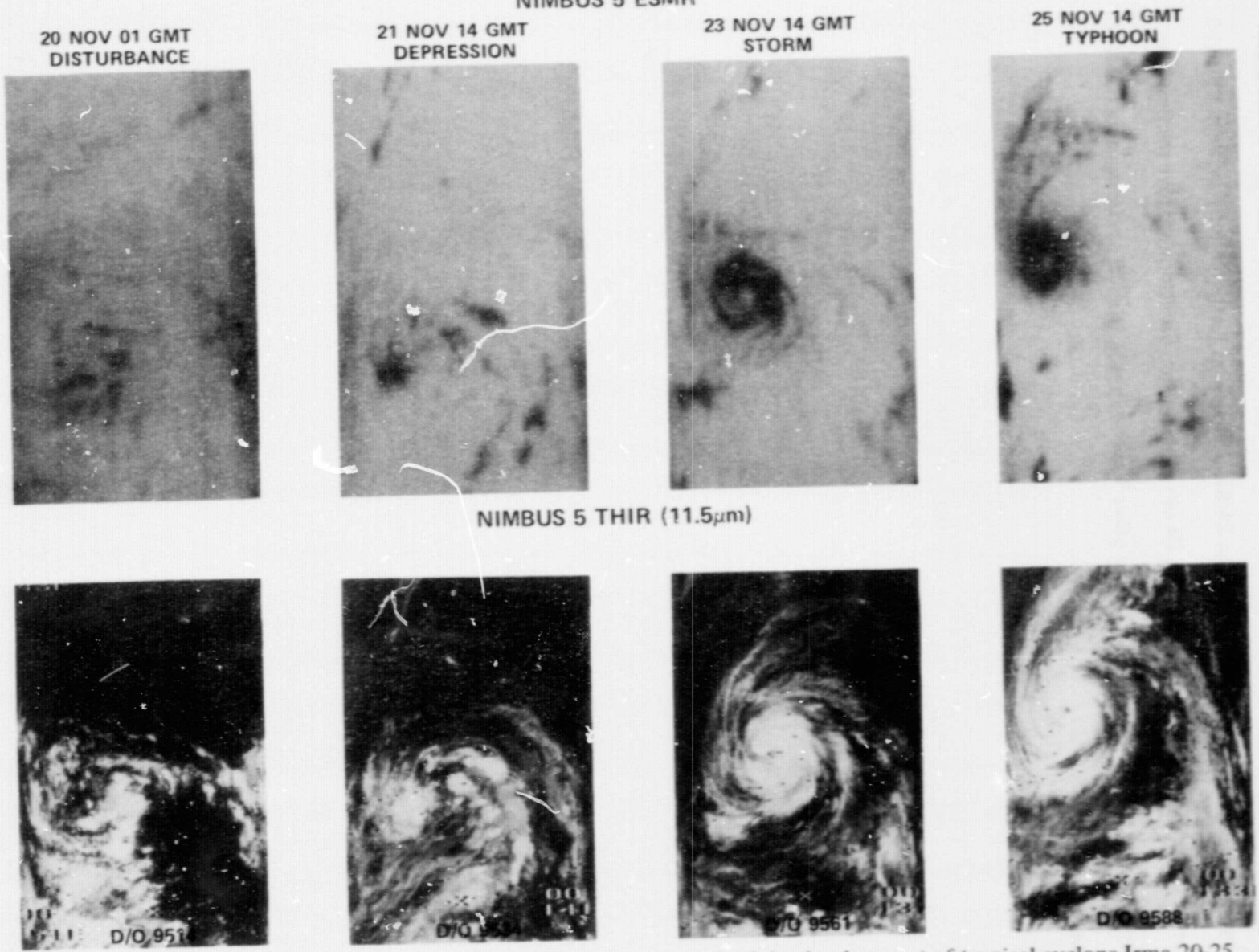

Figure 1. Nimbus 5 EMSR (19.35 GHz) imagery (194 to 226 K gray scale) of the development of tropical cyclone Irma 20-25 November, 1974 (top); Nimbus 5 THIR (11.5 μm) imagery of Irma at the same times (bottom). D/O is the data readout orbit.

identification of a rain free eye region during Irma's tropical storm stage. The eye became more apparent later in the THIR image. Thus, the EMSR-5 images, at least qualitatively, depict intensification features that are not observable in IR or visible images. Similar qualitative relationships were also noted by Allison et al (1974) for other Western Pacific tropical cyclones using ESMR-5 images.

3. DATA PREPARATION AND CALCULATION METHOD

a. Brightness Temperature-Rainfall Relatively

Wilheit et al. (1977) derived an ESMR-5 T_B-rainfall relationship for 19.35 GHz using a radiative transfer model. The model assumes a Marshall-Palmer drop size distribution and limits the vertical extent of the rain to the height of the 0°C isotherm (freezing level height). A layer of 25×10^{-3} g cm^{-3} liquid water content (LWC) is assumed for 0.5 km thickness just below the freezing level. A relative humidity profile linearly decreasing from 100 percent at the freezing level to 0 percent at the surface is used. Upwelling radiance is then calculated for various rainfall rates and for various freezing level heights. The calculated radiance, convertible to T_B, also contains the implicit assumption that, from a satellite data perspective, the IFOV is filled with rain at a constant rainfall rate. The beam filling problem, the lack of knowledge of the depth of rain, and lack of information on amount of cloud LWC and water vapor contribute to errors and uncertainties in estimating rainfall rate from ESMR-5 T_B values (Lovejoy and Austin, 1980).

One problem in estimating rainfall rate from the satellite T_B values is that there are no direct measurements of rain depth, cloud liquid water, and water vapor. In addition, preliminary calculations by the authors indicated that total storm rainfall calculated using the model-derived relationship for the appropriate freezing level heights gave values systematically too low in comparison with previous studies (see section 4a). This was true even for cases of typhoons where the scale of the precipitation was large enough so that the field of view problems were minimized. In order to avoid these problems, an empirical relationship derived by comparing ESMR-5 T_B values with radar-estimated rainfall rates was used. This empirical relationship helped to verify the theoretical results from the microwave radicitive transfer model (Wilheit et al.,1977).

The ESMR-5 T_B -radar comparisons were made for four days during June and July, 1973 and 1974 of disturbed weather in which synoptic scale rain was falling over an ocean background off the Florida coast. The rain rates in these disturbances were measured by a calibrated digitized National Weather Service WSR-57radar at Miami. The rain systems being observed by the ESMR-5 and the radar had many features in common with the disturbances and depressions observed in the Western

Pacific. The average temperature (the average freezing level is approximately 4.5 km) and moisture profile for the rain-comparison cases used were quite similar to what is found in the average Western Pacific disturbance and depressions (Gray et al., 1975). The freezing level height is not a very good measure of effective rainfall height, especially in convective situations where liquid water droplets can exist at temperature at least as cold as -10 to-15C. However, the freezing level height may be a good relative measure of effective rainfall height averaged over a large area (such as a tropical disturbance or typhoon). Since the thermodynamic properties areas appear similar, the assumptions that the rainfall characteristics (e.g., LWC, rain rates, height of the effective rain layer) are similar appears justifiable. Therefore, an empirical relation derived from a data set taken under similar environmental conditions should be valid for use in calculations of rainfall for Western Pacific ocean disturbances. Fig. 2 shows a least squared fit (dashed line) to the radar ESMR-5_B comparison data for rain rates up to 10mm h^{-1} (standard error of estimate is 1.3mm h^{-1}). Because of the larger backscatter from large rain drops at rain rates greater than 10mm h^{-1} ,ESMR-5 T_B values greater than 260K have never been observed over ocean areas. For this reason, the curve was not extrapolated past 10mm h^{-1} . Although this rain rate does not seem equal to the heavy rain rates observed in tropical cyclones, the ESMR-5 estimate is a mean for an area $\geq$600 km^2.

However, to estimate rain rate in Western Pacific typhoons where the average freezing level is approximately 5 km (Frank, 1977; Bell and Kar-sing, 1973), the height of the effective rain layer probably is higher. Since there are no simultaneous ESMR-5 T_B and radar measurements of rain rate in Western Pacific typhoons, the derived empirical relationship (dashed line, Fig. 2) is adjusted according to calculations of Wilheit et al. (1977).

Since the observed difference in the freezing level height between disturbances and typhoons is 0.5 km, we also assume a 0.5 km average rainfall depth difference. To account for this difference in rainfall depth in the ESMR-5 T_B-rainfall rate relationship, the original curve (dashed) in Fig. 2 is shifted by 8K to produce the solid line in Fig. 2. This offset was obtained by extrapolating half the difference in the theoretical calculation for freezing levels of 4 km and 5 km by Wilheit et al. (1977).

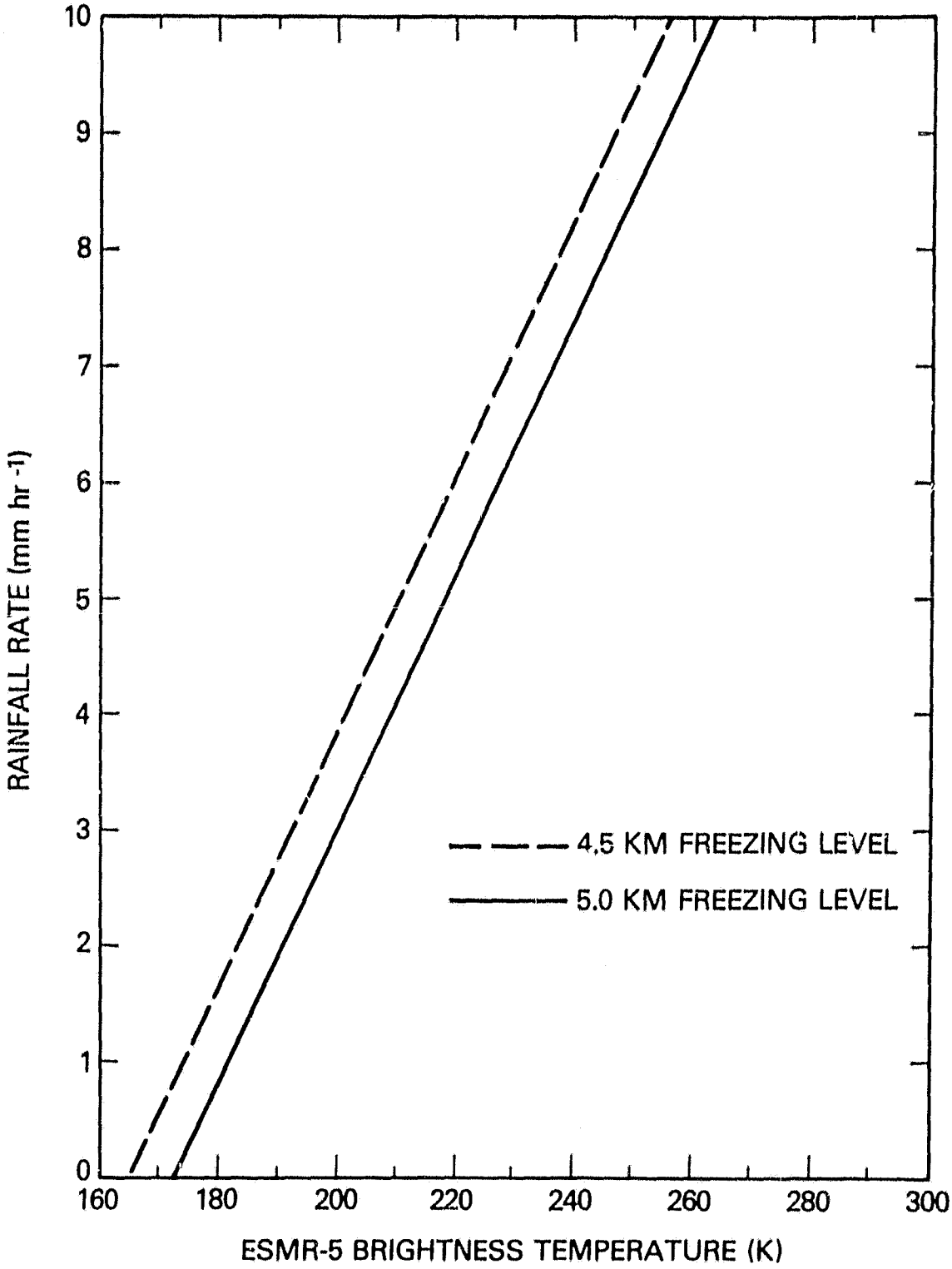

Figure 2. Rainfall rate as a function of Nimbus 5 ESMR brightness temperature (T_B) for the empirical study whose average freezing level is 4.5 km (dashed) and the theoretically adjusted curve for a 5.0 km freezing level (solid).

The use of this 5 km curve (solid line, Fig. 2) in the subsequent calculation for typhoon Nora (1500 GMT 5 October, 1973) produces a value of storm LHR approximately 15 percent larger than the curve used by Adler and Rodgers (1977).

The empirical approach also helps alleviate the field of view problem. The radar-estimated rainfall rate values were available with a much higher horizontal resolution than the ESMR-5 data. Each satellite data point is compared to the average rainfall rate within the ESMR-5 IFOV rather than assuming a constant rainfall rate over the area as was done in the model calculations.

The final validation of this technique will be the comparison of calculated storm rainfall with previous estimates used by other means (see section 4a).

b. Method of Calculation

After a small adjustment to the T_B for scan angle and diurnal variation (Adler and Rodgers, 1977), rain rate for each scan point of each satellite pass confined to a circular area of 444 km radius centered either at the tropical cyclone center of circulation or on the point of maximum ESMR-5 T_B was computed using the adjusted empirical curve in Fig. 2 (solid line). The center of circulation was based on the microwave image and concurrent THIR image, and storm location from the 1973, 1974, and 1975 Annual Typhoon Report. The center of circulation is usually well defined in the microwave data for more mature systems (i.e., see Fig. 1). For disturbances and depressions, a center of circulation is less discernible in the images and usually not documented in the Annual Typhoon Report. For these reasons, a second center of calculation is defined on the point of maximum ESMR-5 T_B. However, for the weaker systems as well as the stronger systems, LHR calculations were found to be approximately the same using both technique for defining the center. Therefore, no further reference will be made to ESMR-5 derived rainfall parameters using maximum ESMR-5 T_B as the center.

For disturbances and depressions, the rainfall rate was also calculated using the ESMR-5 T_B-radar empirical relationship (dashed line, Fig. 2), since the thermodynamics of the cases used for the empirical study were similar to that of the Western Pacific disturbances and depressions. No spatial

variation of thermodynamic and height of the effective rain layer was considered even for mature storms when substantial horizontal gradients are present near the center.

The latent heat release (LHR) over an area is given by

$$LHR = L\rho \int_A R\, da$$

where ρ is the density of the rain (assumed to be equal to 1.0×10^3 km^{-3}), L the latent heat of condensation (2.5×10^{-6} Jkg^{-1}), da the incremental area, and A the area of integration. The integration is performed over circular areas of radii are 111, 222, 333, and 444 km from the center of circulation. As previously mentioned, the rainfall rate R was determined from the rainfall rate and T_B empirical relationship (Fig. 2). In addition to storm LHR calculations, the radial and azimuthal distributions of rainfall rate and the fraction of rainfall contributed by rain rates greater than 5 mm h^{-1}, hereafter called the precipitation intensity parameter (PIP), is also examined in reference to tropical cyclone intensity and direction of motion.

Adler and Rodgers (1977) discussed sources and possible magnitude of the errors affecting the ESMR-5 derived rainfall parameters. Because of the sensitivity of the absolute values of these rainfall parameters to possible errors, the emphasis in this paper is on relative changes with time and on spatial variations in the same storm.

c. Case Studies

Names of the Eastern and Western Pacific Ocean tropical cyclones and times and dates of observations by ESMR-5 are indicated in Table 1. Maximum surface wind speed and information on whether these storms were small (as measured in terms of the outer closed surface isobar surrounding the tropical cyclone) as defined in the Annual Typhoon Report are also given in the table. No attempt was made to include North Atlantic tropical cyclones due to the lack of ESMR-5 observations caused by a satellite interrogation problem over the Atlantic Ocean and the small number of tropical cyclones during the years ESMR-5 was operating. The sample of ESMR-5 observations of the

Western Pacific Ocean tropical cyclones in this study was restricted to an area located between the equator and 25°N and east of 125° E. This eliminated storms which have recurved or crossed the Phillippine Islands. Over both the Eastern and Western Pacific Oceans, a restriction was made on the width of the ESMR-5 swath that was used in each observation. As previously mentioned only storms that fell within 40° of nadir (approximately 1700 km ground swath) were used. This allowed some storm observations to be lost between swaths. Since ESMR-5 was operational only part of the time between December 1972 and January 1975 and because of the narrow swath and imposed restriction, only 71 ESMR-5 tropical cyclone observations were available (49 Western Pacific and 22 Eastern Pacific) for this study.

TABLE 1

WESTERN PACIFIC TROPICAL CYCLONES

NAME	DATE	TIME	Vmax (ms^{-1})	COMMENT
		1973		
Typhoon Billie	14 July	1500 GMT	46	
Depression Ellen	17 July	1500 GMT	<15	
Disturbance Marge	10 September	0200 GMT	<15	Small
Depression Patsy	6 October	1400 GMT	15	Small
Storm Patsy	7 October	0200 GMT	17	Small
Typhoon Patsy	9 October	0200 GMT	40	Small
Disturbance Nora	29 September	1400 GMT	<15	
Disturbance Nora	30 September	0200 GMT	<15	
Disturbance Nora	1 October	1400 GMT	<15	
Depression Nora	2 October	0200 GMT	<15	
Storm Nora	3 October	1500 GMT	31	
Typhoon Nora	5 October	1500 GMT	72	
		1974		
Storm Agnes	24 September	1300 GMT	20	
Typhoon Agnes	26 September	1300 GMT	32	
Typhoon Agnes	27 September	0100 GMT	35	
Disturbance Bess	7 October	1400 GMT	<15	
Storm Bess	8 October	1500 GMT	17	
Storm Bess	9 October	0300 GMT	20	
Storm Carla	4 May	1500 GMT	30	
Disturbance Carmen	13 October	1500 GMT	<15	
Disturbance Dinah	6 June	1400 GMT	<15	
Depression Dinah	7 June	1500 GMT	15	
Storm Della	21 October	0300 GMT	<15	
Disturbance Gilda	26 June	1300 GMT	<15	
Disturbance Gilda	28 June	1400 GMT	<15	
Disturbance Gilda	29 June	1500 GMT	<15	
Storm Gilda	1 July	1500 GMT	22	
Storm Gilda	2 July	0300 GMT	31	
Typhoon Gilda	4 July	0300 GMT	41	
Depression Gloria	2 November	1400 GMT	<15	
Typhoon Gloria	4 November	1400 GMT	45	
Typhoon Gloria	5 November	1500 GMT	42	
Storm Ivy	18 July	1500 GMT	30	
Disturbance Irma	17 November	1400 GMT	<15	
Disturbance Irma	19 November	1400 GMT	<15	
Disturbance Irma	20 November	0200 GMT	<15	
Depression Irma	21 November	1400 GMT	15	
Storm Irma	23 November	1400 GMT	30	

TABLE 1 Cont:

NAME	DATE	TIME	Vmax (ms^{-1})	COMMENT
Typhoon Irma	25 November	1500 GMT	47	
Typhoon Irma	26 November	0200 GMT	55	
Typhoon Irma	26 November	1600 GMT	57	
Depression Polly	25 August	0100 GMT	12	
Storm Polly	26 August	1400 GMT	20	
Storm Polly	27 August	0200 GMT	27	
Typhoon Polly	28 August	1400 GMT	45	
Disturbance Shirley	2 September	1600 GMT	<15	Small
Disturbance Shirley	3 September	1500 GMT	<15	Small
Depression Shirley	4 September	0300 GMT	15	Small
		1975		
Depression Lola	21 January	1400 GMT	<15	
		EASTERN PACIFIC TROPICAL CYCLONES		
		1973		
Disturbance Doreen	16 July	1900 GMT	<15	
Storm Doreen	18 July	1800 GMT	27	
Hurricane Doreen	19 July	1900 GMT	37	
Hurricane Doreen	21 July	0800 GMT	40	
Hurricane Doreen	21 July	2000 GMT	40	
Hurricane Doreen	23 July	0800 GMT	35	
Hurricane Doreen	23 July	2000 GMT	37	
Hurricane Doreen	30 July	1000 GMT	40	
Hurricane Doreen	30 July	2200 GMT	42	
Disturbance Katherine	29 September	0700 GMT	<15	
Storm Katherine	29 September	1800 GMT	17	
Hurricane Katherine	1 October	1900 GMT	45	
Hurricane Katherine	3 October	0800 GMT	42	
Hurricane Katherine	3 October	1900 GMT	40	
Storm Katherine	4 October	0800 GMT	30	
Storm Katherine	4 October	2000 GMT	20	
Depression Katherine	6 October	2100 GMT	15	
		1974		
Disturbance Ione	19 August	2000 GMT	<15	
Storm Ione	23 August	0900 GMT	22	
Storm Ione	23 August	2100 GMT	30	
Hurricane Ione	25 August	0900 GMT	47	
Storm Ione	27 August	0900 GMT	20	

4. RESULTS

a. ESMR-5 derived rainfall parameters compared to previous studies

The average ESMR-5 derived rain rate for 12 observations of Western Pacific typhoons for areas of 111, 222, 333, and 444 km radius from the center of circulation as compared to calculation of previous studies is seen in Table 2. Other than Miller (1958) and Frank (1977), all estimates of mean rain rate are based on the moisture budget technique. The quantities in the table for Miller (1958) were estimated from his table of composite rainfall for 16 hurricanes over Florida, corrected for wind effects. Frank (1977) composited Western Pacific island rainfall for typhoons during the past 21 years.

There is only partial agreement among the estimates in Table 2. Within 111 km radius from the center, the ESMR-5 value is lower than the other studies by as much as a factor of three. However, of the twelve typhoon observations, typhoons Irma and Nora's rain rates (~7 mm h^{-1}) were only a factor of two less than that of three of the other studies, and comparable to the Hawkins and Rubsam (1968) study. Part of the underestimation is due to the saturation of the ESMR-5 sensor at approximately 10 mm h^{-1}. At the 222, 333, and 444 km radii the agreement is better.

The average LHR within 444 km of the center of circulation derived from ESMR-5 for 12 observations of Western Pacific typhoons is 8.7×10^{14} W. This is comparable to LHR calculations using numerical models of mature hurricanes. Kurihara (1975) computed 4.7×10^{14} W for a radius of 500 km from his axisymmetric model; Tuleya and Kurihara (1975) calculated 5.8×10^{14} W for a radius of 500 km from his three-dimensional model; and Anthes (1972) calculated 12.6×10^{14} W for the domain of his asymmetric hurricane.

For 15 observations of Western Pacific disturbances the mean rain rate for an area of 444 km radius from the center of circulation was 0.7 mm h^{-1}, based on the ESMR-5 data. Williams and Gray (1973) indicated a value of 1.0 mm h^{-1} for a 444 km square over composited

cloud clusters while Zehr (1976) estimated a value of 0.9 mm h^{-1} for cloud clusters over a circular area of radius 444 km. However, using the empirical curve that relates ESMR-5 T_B to rain rate (dashed curve, Fig. 2) in raining atmospheres found in Western Pacific disturbances (Gray et al., 1975), a value of 1.1 mm h^{-1} is derived which is closer to the findings from previous studies. Thus, it is seen that the ESMR-5 derived rain rate/LHR values for both the disturbance and typhoon stage compare reasonably well with previous estimates. The results also indicate that mature hurricanes and typhoons have approximately twice as much LHR or rainfall as do tropical disturbances.

TABLE 2

MEAN RAIN RATE COMPARISONS FOR MATURE STORMS (mm h^{-1})

	Radius of Area Covered (km)			
	111	222	333	444
Present study (Western Pacific Typhoons)*	4.2	3.4	2.4	1.9
Hughes (1952) (composite)	14.0	4.5	2.1	1.2
Palmen and Riehl (1957) (composite)	–	5.3	–	–
Miller (1958) (composite)	–	4.6	–	1.8
Riehl and Malkus (1961) (Daisy, 1958)	13.6	–	–	–
Miller (1962) (Helene, 1958)	13.9	–	–	–
Hawkins and Rubsam (1968) (Hilda, 1964)	6.3	–	–	–
Frank (1977) (composite)	–	3.9		2.2

*Average of 12 observations

b. Case Studies

Successive ESMR-5 passes over four Eastern and Western Pacific Ocean storms afford the opportunity to examine the relative change in the ESMR-5 derived rainfall parameters as they relate to changes in tropical cyclone intensity. Examining the relative change rather than the absolute value of these ESMR-5 derived rainfall parameters is particularly valuable because it mitigates the sensitivity caused by the errors described by Adler and Rodgers (1977). Four tropical cyclones will be examined (3 Western Pacific and 1 Eastern Pacific) emphasizing the LHR, radial distribution of rainfall and the precipitation intensity parameter (PIP). These storms have been selected because they have the most complete set of ESMR-5 observations.

(i) Irma (Western Pacific, 17-26 November, 1974)

Figure 3 displays the LHR and other rainfall parameters as a function of time for tropical cyclone Irma. During the time period examined, Irma developed from a disturbance north of Truk Island to a typhoon before crossing the Philippine Islands on 27 November, 1973. Four curves are shown. The solid curves show the LHR derived from the 5 km freezing level rainfall rate and T_B relationship (solid curve, Fig. 2) for circular area's of 222 km (lower values) and 444 km radius. The dashed curve shows the LHR derived from the 4.5 km freezing level rain rate and T_B relationship (dashed curve, Fig. 2) for the same circular areas. At the top of the figure are shown the maximum winds (ms^{-1}) derived either from reconnaissance aircraft or the DMSP satellite images using the Dvorak (1975) technique and the central pressure (mb) derived from reconnaissance aircraft (U.S. Fleet Weather Center/Joint Typhoon Warning Center, 1974). The number in the parenthesis associated with the solid LHR curve derived for a circular area of 444 km are the PIP values.

Calculations of LHR were made from ESMR-5 data at eight different times during the period. The number of ESMR-5 observations of tropical cyclone Irma as well as the other storms that will be examined in this section were limited due to missing orbits and because the storm was sometimes located between adjacent orbital scans.

From 17-21 November, before Irma was classified as a depression, the LHR and PIP values for a circular area 444 km in radius using the 5.0 km freezing level ESMR-5 T_B curve were low ($<3.1 \times 10^{14}$ W and <.25 respectively). However, using the 4.5 km freezing level ESMR-5 T_B and rain rate curve (dashed curve, Fig. 2) which is more representative for weak systems (Gray, et al., 1975), the LHR values are nearly doubled (dashed lines). These LHR values are closer to the values found in earlier studies (see previous section). The results displayed in Fig. 3 indicate increasing LHR accompanying intensification irrespective of which set of curves (dash or solid) are used for the earlier stages. This was true for all cases that were examined. However, since there is no information available about the thermodynamics of these storms, the calculations based on the 5.0 km freezing level for the ESMR-5 and T_B rain rate curve (solid curve, Fig. 2) will be emphasized in the following discussion of relative changes.

As was mentioned previously, the CISK mechanism does not necessarily operate under conditions of tropical cyclogenesis (Zehr, 1976; Erickson, 1977; and Arnold, 1977). However, during the later stages of tropical cyclone intensification numerical models suggest that the importance of the CISK mechanism becomes greater. Evidence to support this is seen in the case of Irma as well as in the other cases. A trend of increasing LHR is seen after the 19 November. By the 21 November the LHR values had more than doubled for the circular area with radius of 444 km and continued to increase to 9.6×10^{14} W on the 23 November and 11.5×10^{14} W on the 25 November when the LHR reached its maximum. The trend of increasing LHR values appears to begin 2 days prior to when Irma was first classified as a tropical depression (surface wind maximum less than 15 ms^{-1}) on 21 November. This lag is also observed in the other cases.

The Irma intensification during this period is also evident in other ESMR-5 derived rainfall parameters. The PIP value is seen to increase from 0.25 on the 21 November to 0.56 on the 25 November, indicating that approximately half of the storm rainfall is being contributed by rain rates greater than 5 mm h^{-1}. There is also a concentration of rainfall towards the inner part of the storm. The fraction of the storm rainfall within 222 km, given by the ratio of the LHR value in the lower

solid curve to the corresponding value in the upper solid curve, goes from 0.41 on 21 November to 0.61 on the 25 November. The concentration of Irma's rainfall towards the center of circulation is also seen qualitatively in the ESMR-5 images in Fig. 1.

Fig. 4 further demonstrates the radial distribution of rain rate as well as the increase in rain rate as it relates to Irma's intensification. The figure shows the mean rainfall rate as a function of distance from the center of circulation of Irma at various stages of development. It is seen that as Irma intensifies, the average rain rate increases and the radius of maximum rain rate moves towards the center of circulation. Rain rates increase from a maximum of 2.0 mm h^{-1} at depression stage to 5.5 mm h^{-1} at storm stage to 8.0 mm h^{-1} at typhoon stage. The radius of maximum rain rate decreases from 138 km during storm stage to approximately 100 km during typhoon stage. During the depression stage, the center of circulation was not well defined and the radius of maximum rain rate may not be as meaningful. Minimum rain rate nearer the center of circulation is indicative of the light rain rates within the eye of the storm. Thus, it is observed that the intensification of Irma with maximum winds increasing from 15 m s^{-1} to 50 m s^{-1} occurs with increasing LHR, concentration of rainfall towards the center of the storm, and an increasing contribution of heavier rain rates to the storm rainfall.

Typhoon Irma has its maximum satellite-observed LHR and PIP values at 15 GMT 25 November. In the next two observations there is a slight decrease in storm LHR and a lowering of the PIP value. These changes, if real, are indicative of a slight weakening of the storms transverse circulation. However, the surface pressure apparently continues to decrease to 939 mb before intensifying slightly. This sequence of events is consistent with a time lag between maximum rainfall and maximum storm intensity. Observation of this lag is supported by the numerical model calculation of Rosenthal (1978). His model showed that maximum vertical motion preceded minimum pressure by 24 to 36 h. Gentry et al. (1980) also observed for 5 storms a lag of 24 to 36 h between the time at which the minimum cloud top temperatures were observed by the Nimbus-4 THIR 11.5 μm channel and the time that a cyclone had its highest winds.

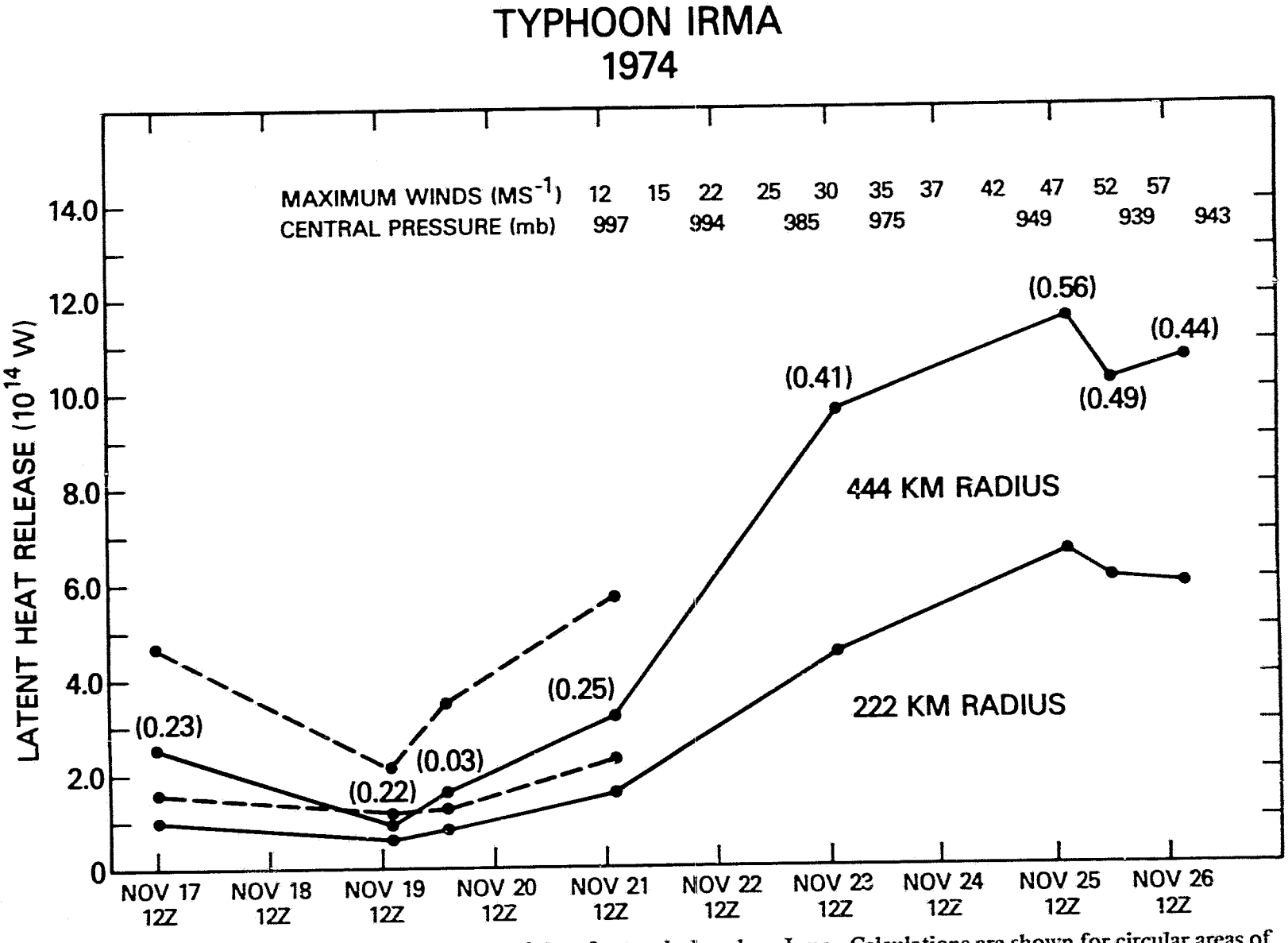

Figure 3. Latent Heat Release (LHR) as a function of time for tropical cyclone Irma. Calculations are shown for circular areas of 222 km and 444 km radius for freezing levels 4.5 km (dashed) and 5 km (solid). Numbers in parentheses are fractions of rainfall contributed by rainfall rates greater than 5 mm h^{-1}.

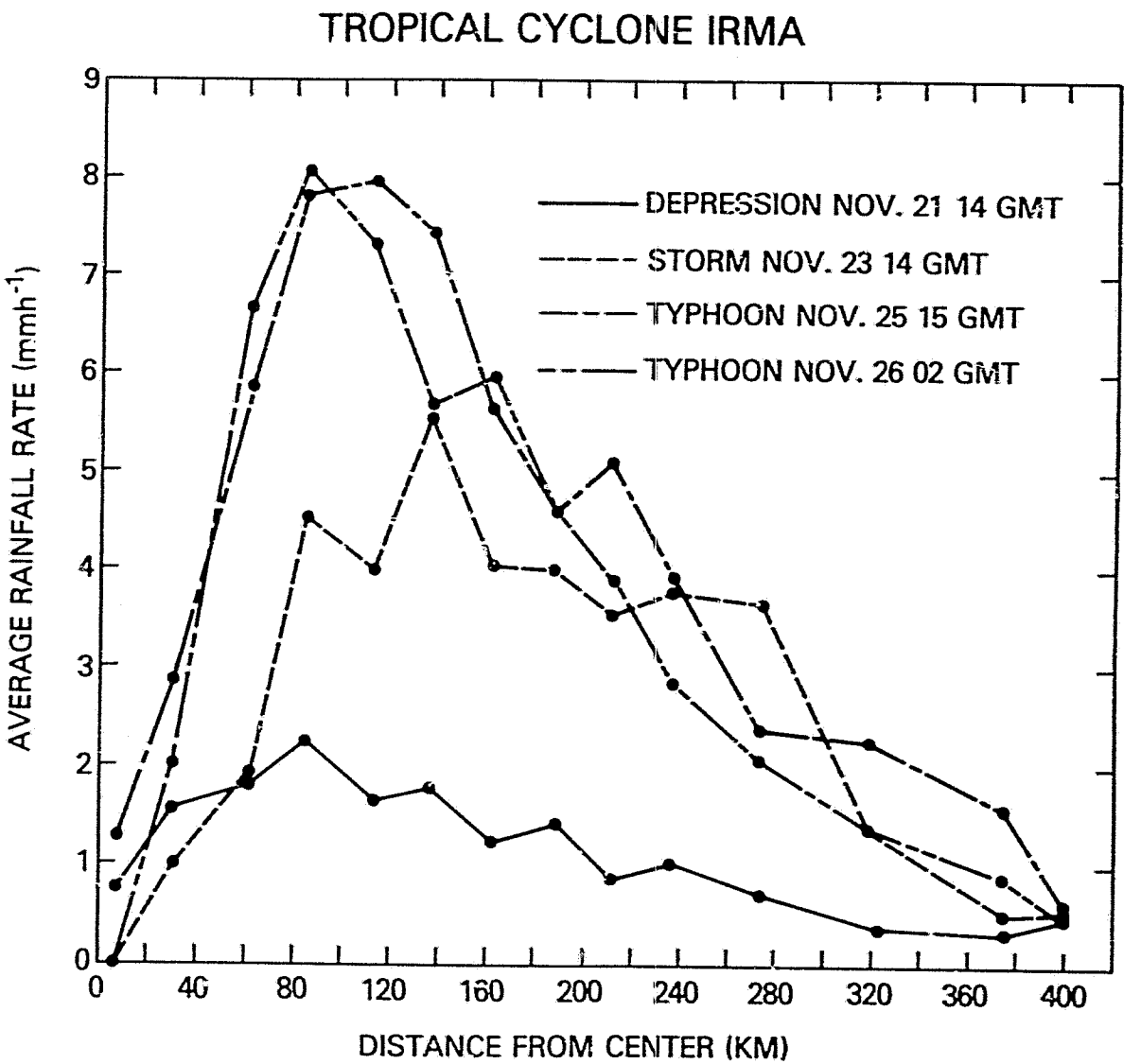

Figure 4. Mean rainfall rate as a function of radial distances from the storm center for four observations of Irma as the storm intensified.

(ii) Gilda (Western Pacific 26 June – 5 July, 1974)

Gilda was first detected as a disturbance at approximately 18°N 160°E on 25 June, 1974 and continued its disturbance status until 30 June. The system gradually intensified as it moved in a westward direction until 2 July. At this time it reached typhoon strength and moved in a more northerly direction (U.S. Fleet Weather Center, Annual Typhoon Report, 1974). The LHR and the PIP values before 29 June as seen in Fig. 5 were low ($\leq 2.2 \times 10^{14}$ W, $\leq .23$ respectively). The first indication of an upward trend of LHR is after 29 June. Exact timing of the initialtion of this trend cannot be given because of the limited number ESMR-5 observations; however, it appears to occur before intensification was indicated by reconnaissance aircraft. Between 29 June and 1 July, LHR values for a circular area of radius of 444 km using the 5.0 km freezing level ESMR-5 and T_B rain rate relationship increased from 1.5×10^{14} W to 6.8×10^{14} W while the PIP increased from 0.06 to 0.47. During 1 July, two ESMR-5 observations were made at approximately at 06 and 18 Local Standard Time (LST). A decrease in LHR at 18 LST may be attributed to not locating the center accurately but may, be also due to a diurnal oscillation. This fluctuation, if real, is in agreement with the results of Frank (1977). Frank found that from a statistical analysis of rainfall in typhoons obtained from 21 years of hourly rainfall data from various western Pacific islands stations that there appears to be a small diurnal variation in typhoon rainfall with a maximum at approximately 11 LST and a minimum at 18 LST.

After July 1, the storm continued to intensify with maximum winds of approximately 45 m s^{-1} and a minimum pressure of 944 mb on 4 July. ESMR-5 observations early on 4 July showed an increase of LHR to 9.4×10^{14} W but a decrease in the PIP from 0.52 to 0.39. In addition, the fraction of LHR within 222 km of the center of circulation showed a slight decrease from 0.50 to 0.48. To better demonstrate the radial distribution of rain rate as well as the change in rain rate for Gilda as it intensified to typhoon stage, Fig. 6 shows the radial distribution of rain rate for different stages of Gilda's development. It is seen that rain rates increased dramatically at all radial distances as Gilda intensified from a disturbance on the 28 June (maximum rain rate 1.8 mm h^{-1}) to

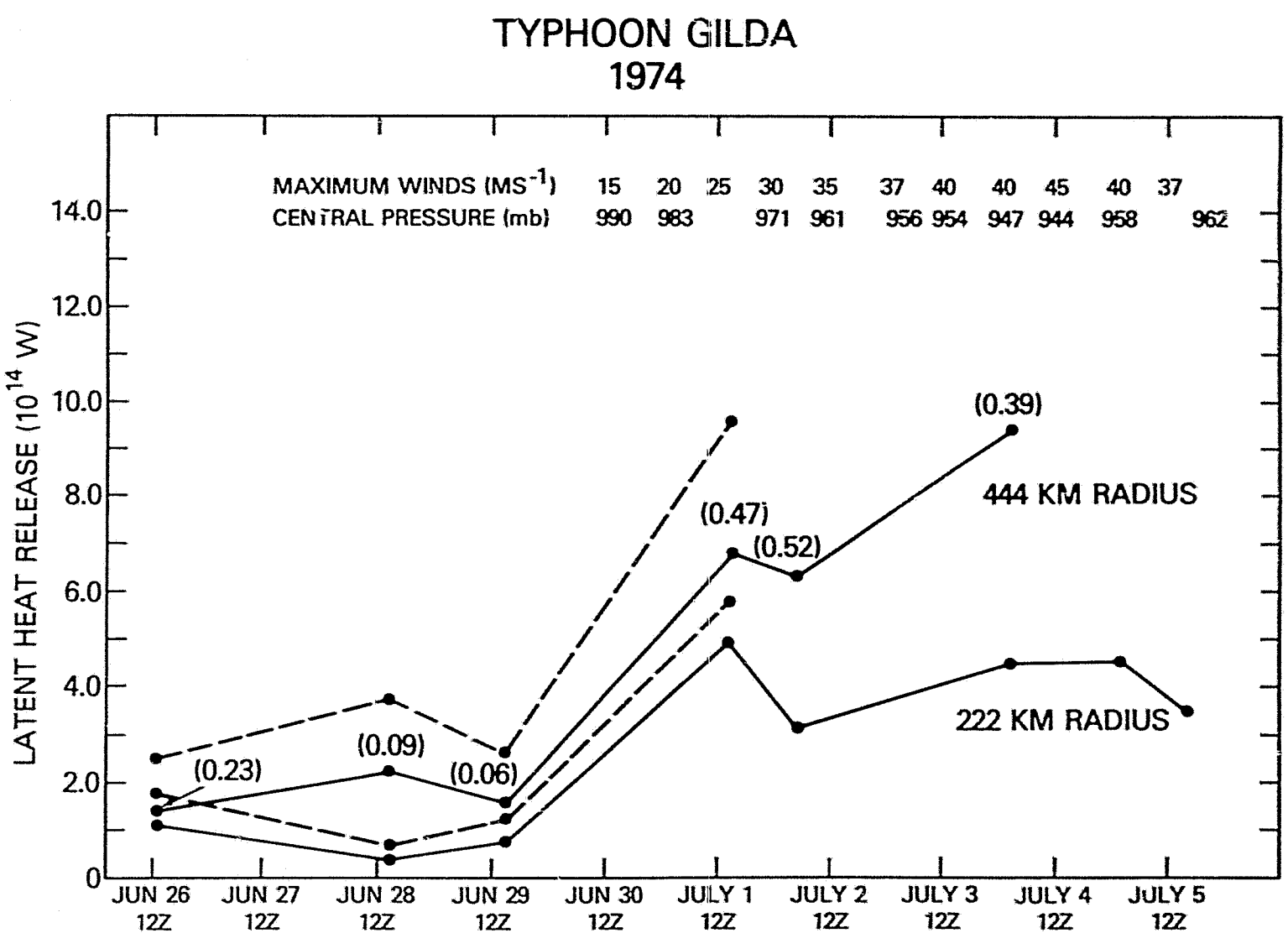

Figure 5. Latent Heat Release (LHR) as a function of time for tropical cyclone Gilda. Otherwise the notation is the same as in Fig.

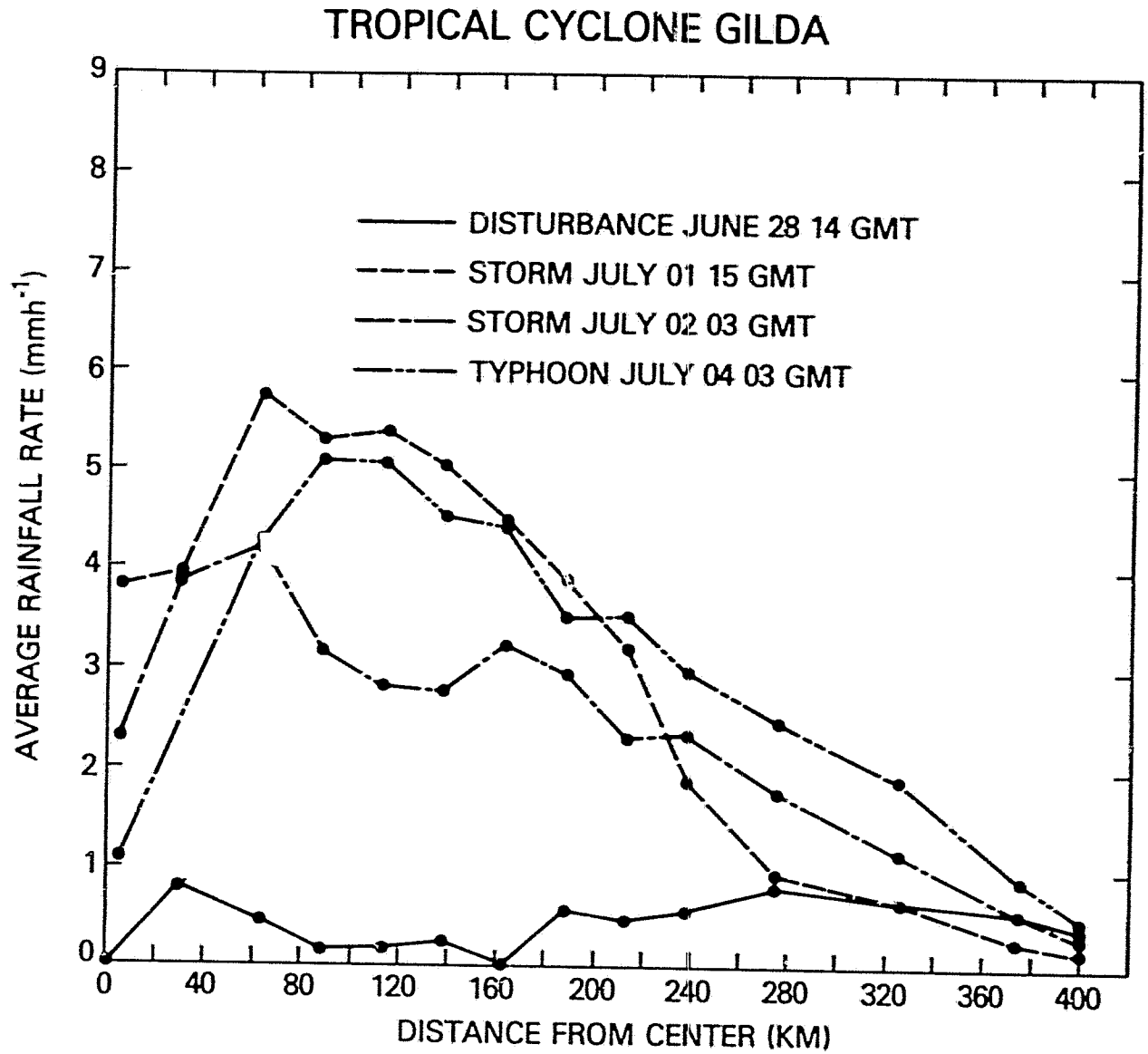

Figure 6. Mean rainfall rate as a function of radial distance from the storm center for four observations of Gilda as the storm intensified.

storm stage on the 1 July (maximum rain rate 5.8 mm h^{-1}). However, as Gilda continued to intensify with maximum wind increasing from 22 m s^{-1} on the 1 July to 31 m s^{-1} on the 2 July, rain rates decrease at all radii inside 238 km from the center probably in response to the diurnal variation. As Gilda further intensified to typhoon stage, rain rate again increased at all radii outside 61 km from the center, although the radius of maximum rain rate increased. Thus, it is observed that although the LHR increased substantially, some of the other rainfall indicators of further intensification are not consistent with the other cases.

The lag between time of maximum LHR and maximum intensity that was observed for Irma is not well defined with Gilda. However, it is suggested in Fig. 5 that at the time the outer portion of the storm began to be affected by land, the LHR within an area 222 km from the center of circulation did not increase further even though Gilda continued to intensify. Because of the lack of ESMR observations between the 2-4 July, the time of maximum LHR may have been missed. The last ESMR observation on 5 July indicates a decrease in LHR which corresponds with the weakening of Gilda.

(iii) Nora (Western Pacific 29 September – 6 October, 1973)

The typhoon Nora case, shown in Fig. 7, has already been discussed in detail by Adler and Rodgers (1977). Although the relative changes in LHR are similar to the calculations in the earlier paper, the absolute values are larger since a different ESMR-5 T_B and rain rate relationship was used. In addition to what was observed by Adler and Rodgers (1977) and is seen in this figure (i.e. LHR and PIP increases and an inward movement of the radius of maximum rain rate are associated with intensification), it is again observed that there is a trend of increasing LHR prior to the time when reconnaissance aircraft first took observations. The lag between the time of maximum LHR and maximum intensity that was observed with Irma was not observed with Nora. This was due to the loss of ESMR-5 data when Nora moved over the Philippine Islands.

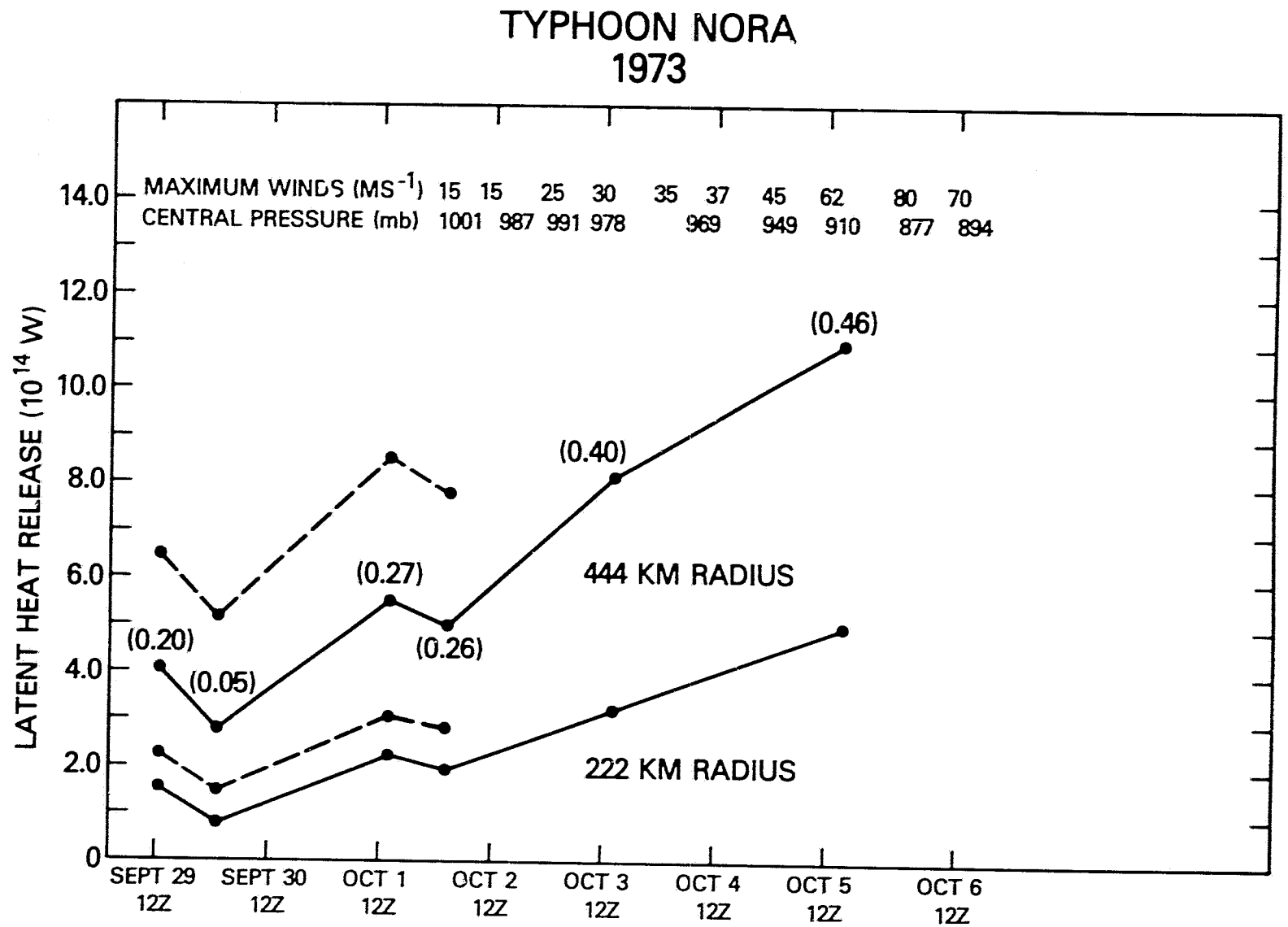

Figure 7. Latent Heat Release (LHR) as a function of time for tropical cyclone Nora. Otherwise the notation is the same as in Fig. 3.

(iv) Doreen (Eastern Pacific, 16–30 July, 1973)

Tropical cyclone Doreen offered an excellent opportunity to examine the relative change in the ESMR-5 derived rainfall parameters and tropical cyclone intensity since Doreen traveled over the open ocean during its entire lifetime. It also offered an opportunity to examine the relative change in the ESMR-5 derived rainfall parameters for a storm that was weakening. As Doreen traveled westward seven ESMR-5 observations were obtained from 16-23 July when Doreen developed from a cluster to hurricane stage and then weakened to storm strength. Two other ESMR-5 observations of Doreen were obtained a week later. The results of ESMR-5 rainfall parameters is seen in Fig. 8.

As was observed with the western Pacific tropical cyclones, an increase in LHR (1.5×10^{14} W to 8.0×10^{14} W) and PIP (0.08 to 0.37) indicated an intensification process and there is a suggestion that this occurred before Doreen became a depression as indicated by U.S. Fleet Weather Central Annual Typhoon Report (1973). There are also strong indications in Fig. 8 that the precipitation parameters peaked 1-2 days before the storm reached maximum intensity. According to the reported "best track" winds (estimated by the Dvorak satellite image technique) the storm had its highest sustained winds on 20-21 July. Minimum sea level pressure occurred about that time, or shortly thereafter. The storm LHR (444 km radius) reached its maximum a day later. The PIP values also peaked on 18-19 July, with the fraction of storm rainfall within 222 km ascending to a value of 0.72 on 19 July. Thus, total storm rainfall and the rainfall concentration parameters appeared to reach their highest values before the storm reached its maximum intensity.

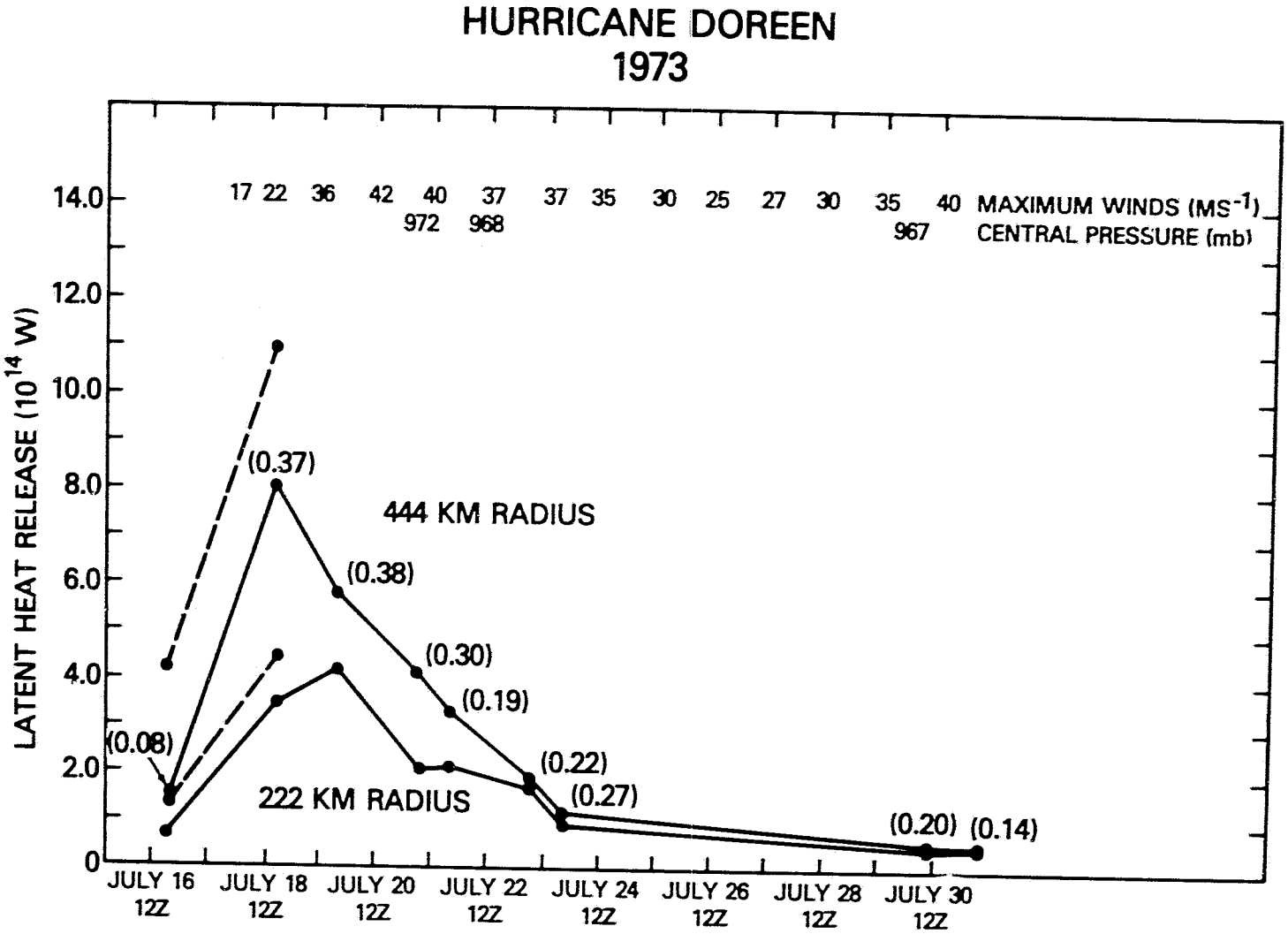

Figure 8. Latent Heat Release (LHR) as a function of time for tropical cyclone Doreen. Otherwise the notation is the same as in Fig. 3.

As Doreen moved over ocean areas whose July mean sea surface temperatures were less than 26°C (Robinson and Bauer, 1971) evidence of weakening was first observed in ESMR-5 derived rainfall parameters. Sea surface temperatures of 26°C are the lowest water temperature for which warm-core cyclones are likely to maintain themselves (Palmen and Newton, 1969). LHR values decreased from a maximum of 8.0×10^{14} W to 1.2×10^{14} W while the PIP decreased from 0.37 to 0.27. A decrease in the concentration of rainfall within 222 km of the center of circulation was also noted after the 19 July, but by 23 July almost all the rain in this small, tight system was within 222 km. An eye is still evident in the accompanying THIR images. The two ESMR-5 observations on 30 July indicated a further decrease in the LHR and PIP values. The reintensification of Doreen on the 27 July as observed in the winds (estimated from DMSP satellite) could not be related to the derived rainfall parameters from ESMR-5 since there were no ESMR-5 observations for a week prior to the 30 July.

c. Summary of Western Pacific Tropical Cyclone Statistics

It can be seen from the individual case studies that intensification can be monitored and possibly predicted through the use of ESMR-5 data. However, in order to obtain a better understanding of the relation of storm intensity to the rainfall parameters calculated from the ESMR-5 data, results for all 17 Western Pacific tropical cyclones (see Table 1) at different intensities were examined. These storms were limited to an open ocean area between the equator and 25°N and east of 125°E for the reasons previously discussed.

(i) LHR

Fig. 9, which shows the relation between intensity (maximum winds ms^{-1}) and LHR for a circular area 444 km in radius, indicates a positive correlation. The cross marks depict tropical disturbances with their intensity arbitrarily plotted at 10 m s^{-1}. Circled crosses and dots depict small storms as reported in the Annual Typhoon Reports. All values are calculated based on the 5 km freezing level relationship. There is a large scatter in the diagrams, but there is still an obvious correlation between storm intensity and storm LHR. Ambiguous results occur, however, when observing small storms. For example, typhoon Patsy (October 9, 1973) had maximum surface winds up to 40 ms^{-1} that corresponded with LHR of only 3.0×10^{14} W.

It was shown from the case studies that the ESMR-5 observations could be used to monitor tropical cyclone intensification prior to the time when the tropical cyclone was first named (storm stage or greater with maximum winds ≥ 17 ms^{-1}) and sometimes prior to the aircraft reconnaissance flights. To illustrate this with the complete Western Pacific tropical cyclone set, Fig. 10 shows the LHR value for each tropical cyclone observation relative to the time when the tropical cyclone was first named. The heavy line in the middle represents this reference time and the negative (positive) numbers represent the number of days prior to (after) the tropical cyclone was named. The dashed line is a subjective fit of the data. The dots represent tropical cyclone observations with maximum winds less than 32 ms^{-1} and the triangles represent tropical cyclone observations with maximum winds greater or equal to 32 ms^{-1}. Circles around triangles and dots indicate small tropical cyclones. All tropical cyclones occuring prior to the time that the tropical cyclone was first named are, of course, less than storm stage.

It is suggested from Fig. 10 that a trend of increasing LHR occurs with time approximately 1 to 2 days prior to being named. Earlier than that the scatter of the LHR observations suggest that there is no trend in the LHR. This again supports the finding that the CISK mechanism may not be important in tropical cyclone genesis, but is important for the intensification process. After the time the tropical cyclone becomes named, LHR is seen to continue to increase with time even

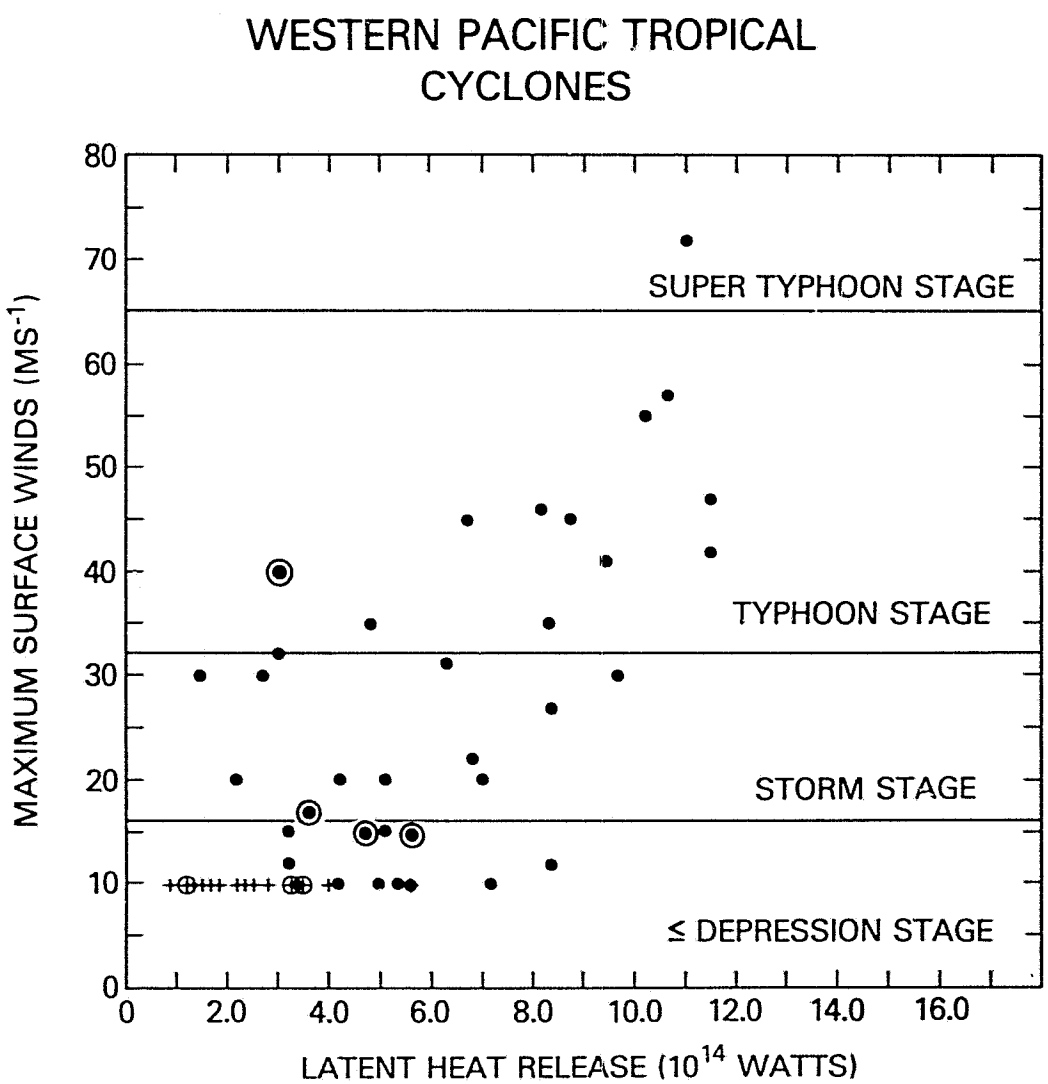

Figure 9. Scatter diagram of storm intensity versus Latent Heat Release (LHR) for Western Pacific ocean tropical cyclones. Crosses indicate tropical disturbances. Circled dots and crosses indicate small storms.

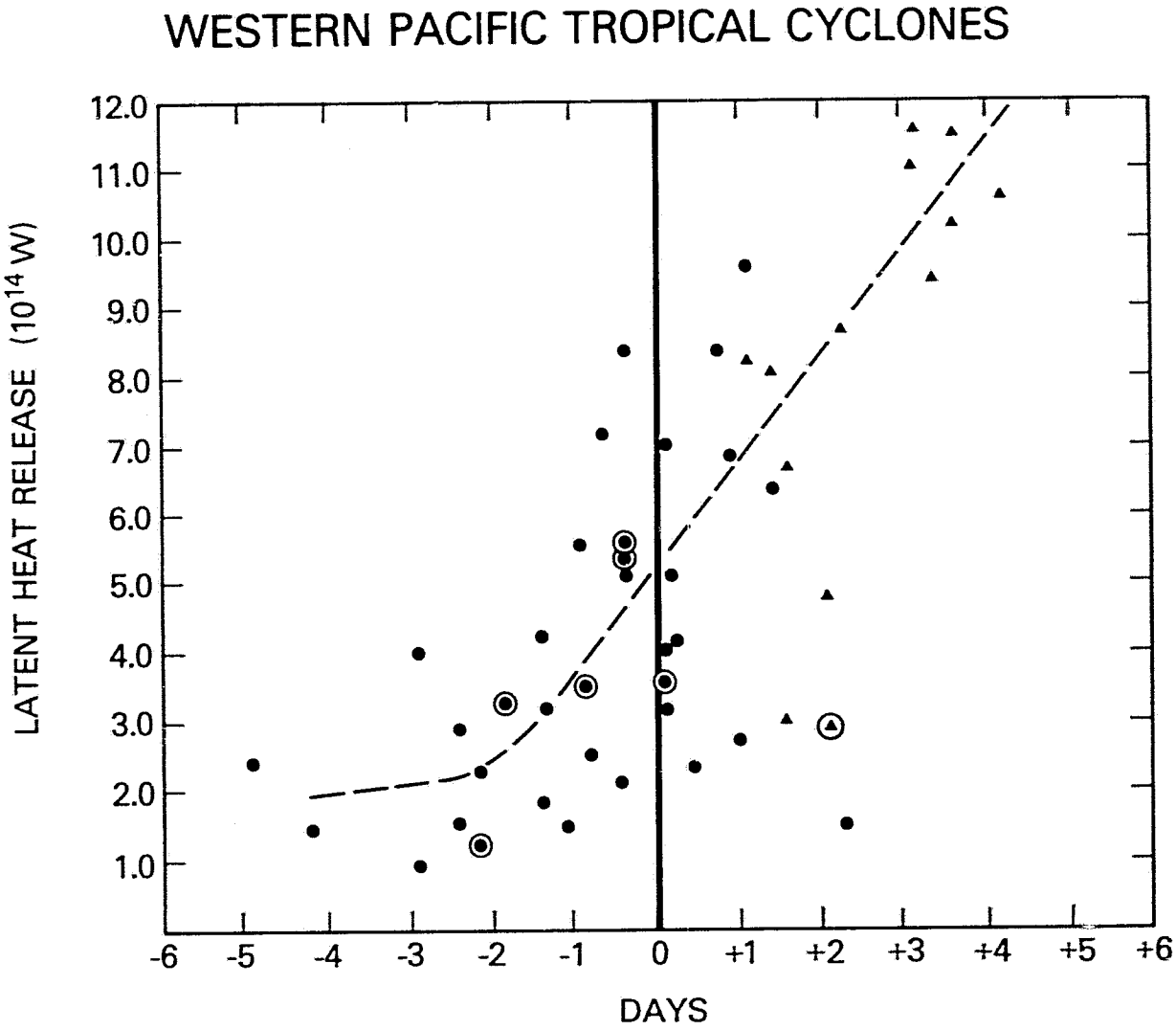

Figure 10. Scatter diagram of Western Pacific ocean tropical cyclone Latent Heat Release (LHR) versus time when the tropical cyclone reaches storm stage. The heavy line in the middle represents the time the tropical cyclone reached storm stage and the negative (positive) numbers represent the number of days prior to (after) the time that the tropical cyclone reached storm stage. Dots (triangles) represent storms with maximum wind < 32 m s^{-1} (≥ 32 m s^{-1}). Circled triangles and dots indicate small storms. The dashed line is a subjective fit to the data.

though there are a few observations (some of which are ESMR-5 observations of small tropical cyclones) that indicate low LHR values. Therefore, it is suggested from this sample of Western Pacific tropical cyclones and from the case studies that ESMR-5 derived LHR observations can be used to help detect tropical cyclone intensification 1 to 2 days prior to storm stage. This information could therefore supplement information obtained from current aircraft reconnaissance flights.

(ii) PIP and Radial distribution of Rainfall

Fig. 11 (same format as Fig. 9) which shows the relation between storm intensity and PIP values indicates a similar positive, but a poorer correlation than that in Fig. 9. For weak systems ($\leq$ depression stage) the PIP average is approximately 0.24 even though there are four values > 0.35. This indicates that the rain in the weak and developing storms is primarily light (rain rates < 5 mmh^{-1}). This does not rule out small, intense showers, but means that on the scale of the IFOV of ESMR-5 (≥ 625 km^2) relatively light rain prevails. For tropical cyclones at stronger intensities the PIP increases from a average of 0.33 at storm stage to a average of 0.39 at typhoon stage (this includes super typhoon Nora). Thus, as the storms intensity more of the LHR is being contributed by rainfall rates greater than 5 mmh^{-1}. Typhoon Patsy (October 9, 1973) the "small" typhoon in Fig. 11 has a PIP value of only 0.16 along with a low value of storm LHR.

The variation of rainfall intensity with storm intensification is also shown in Fig. 12. This diagram shows the distribution of volume rain rate per unit rain rate (units in terms of area) as a function of rain rate for the composite tropical cyclone at four different stages of development. A similar diagram for one storm (Nora, 1973) is shown by Adler and Rodgers (1977). The numbers within the parentheses indicate the number of ESMR-5 observations. This parameter is computed for a circular area of 444 km distance from the center of circulation. The area under the curve is the volume rain rate in the storm, which is proportional to LHR. It is seen that as the composite tropical cyclone intensifies the area under the curve grows indicating rising LHR, and there is also a greater relative contribution to LHR from rain rates larger than 5 mmh^{-1}.

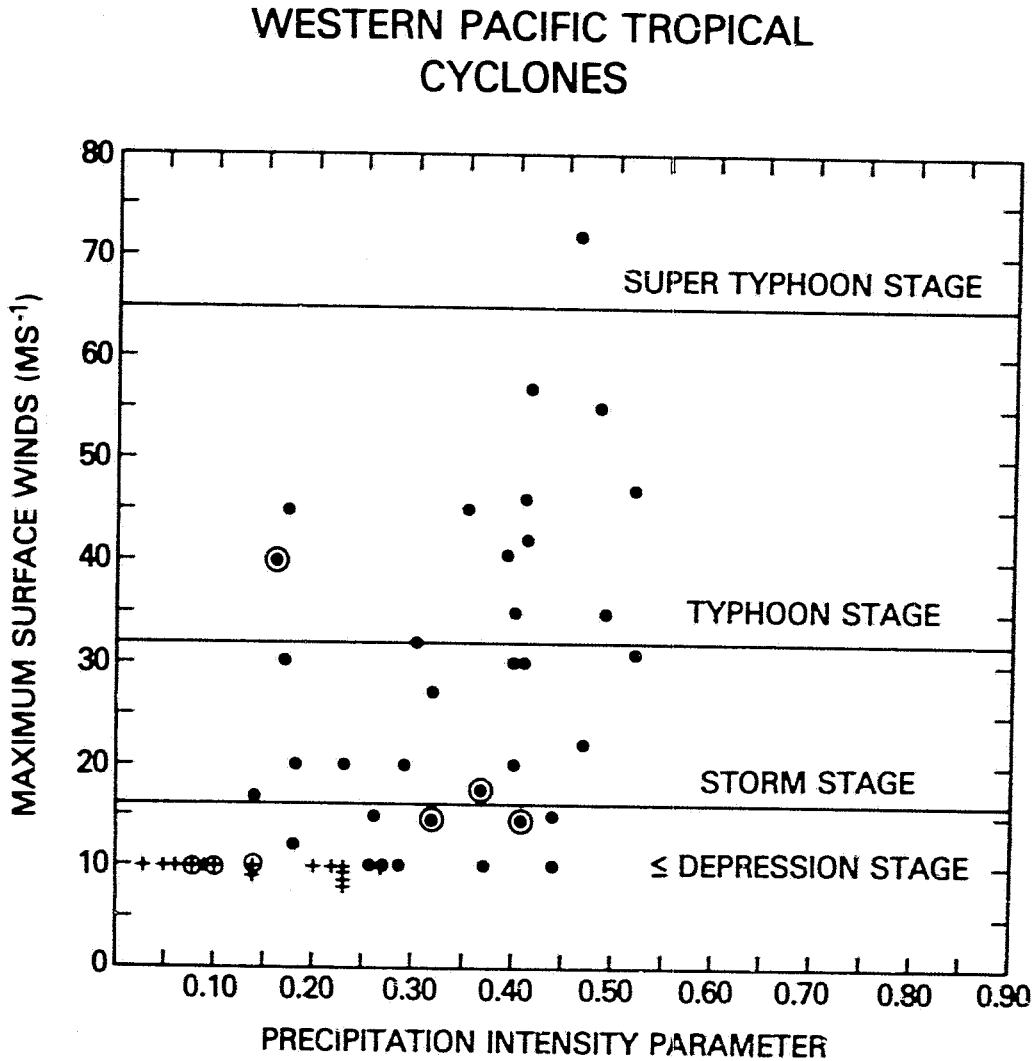

Figure 11. Scatter diagram of storm intensity versus the precipitation intensity parameter (PIP) for Western Pacific ocean tropical cyclones. Otherwise the notation is the same as in Figure 9.

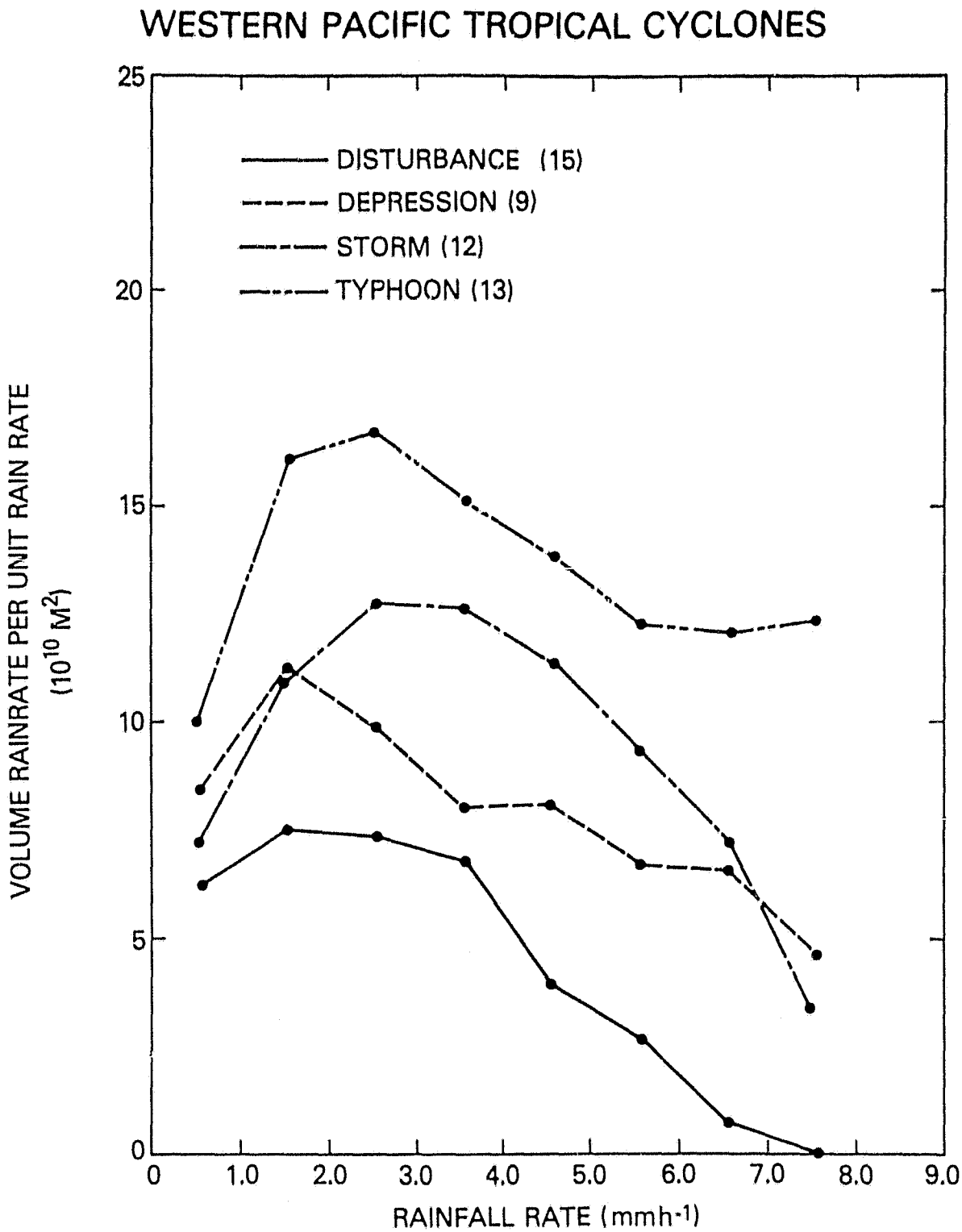

Figure 12. Contribution of various rainfall rate magnitudes to total volume precipitation for Western Pacific ocean tropical cyclones at various stages of development.

Fig. 13 which shows the radial distribution of rain rate for the composite tropical cyclone at different stages of development (similar to Fig. 4 and Fig. 6) illustrates the increase of rain rate with intensification (the number within the parenthesis gives the number of ESMR-5 observations). It is seen that as a tropical cyclone intensifies the rain rate at all distances from the center of circulation increases. At a radial distance of approximately 80 to 100 km from the center of circulation there is a maximum in rain rate for all stages. There is no indication from these curves that the radius of maximum rain rate moves towards the center with increasing intensity, as was observed in most of the case studies. This can be attributed to the averaging process masking this subtle change. However, the contraction of the rain maximum towards the center is weakly observed in the mean fractional amount of LHR within 222 km. This parameter increases from 0.44 at depression stage to 0.51 at storm stage to finally 0.53 at typhoon stage. A decrease was noted as the mean tropical cyclone developed from disturbance 0.47 to depression 0.44 which may due to the difficulty in locating the center of circulation at disturbance stage.

(iii) Azimuthal distribution

The azimuthal distribution of rainfall for the Western Pacific tropical cyclones at all stages was also examined. The rainfall distribution was rotated to a common axis based on storm motion. The results indicate a slight preference for higher rainfall in the right half of the composite storm. Frank (1977) indicated a slight preference for the right-rear quadrant, based on compositing 21 years of hourly rainfall data in typhoons from 9 Western Pacific islands.

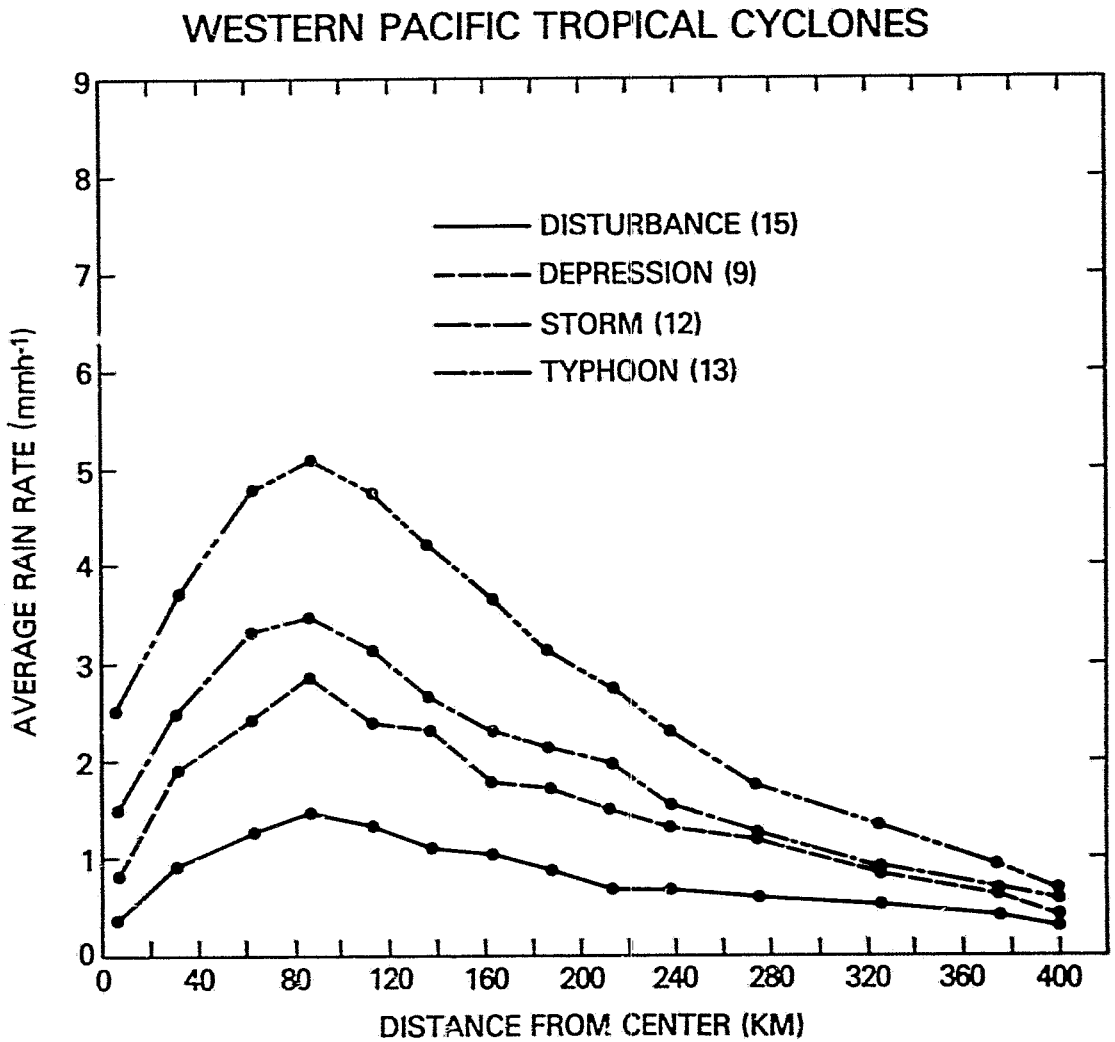

Figure 13. Mean rainfall rate as a function of radial distance from the storm center for Western Pacific ocean tropical cyclones at various stages of development.

d. Comparison of Western Pacific Typhoons with Eastern Pacific Hurricanes

Analysis of ESMR-5 derived rainfall parameters revealed that there are significant differences between Western Pacific typhoons and Eastern Pacific hurricanes for this sample. The comparison of the results for these hurricanes and typhoons is shown in Table 3. Since the average freezing-level for Eastern Pacific hurricanes has not been documented, it is not known whether the Eastern Pacific hurricane freezing level is closer to that of the Western Atlantic hurricane with a freezing level at approximately 4.5 km (Jordon, 1958 and Bell and Karsing, 1973) or with the Western Pacific typhoon with a freezing level at approximately 5.0 km (Frank, 1977 and Bell and Karsing, 1973). Therefore, the Eastern Pacific hurricane's rainfall parameters were computed using both the 4.5 and 5.0 km freezing level ESMR-5 T_B and rainfall rate relationships. However, since the Western Pacific typhoon average freezing level is documented, only the 5.0 km freezing level ESMR-5 T_B and rainfall rate relationship was used to compute the rainfall parameters. The number in parenthesis are the number of observations. The first two lines in the table display the large disparity in total rainfall or LHR between mature systems in the two areas of the oceans for areas of both 222 km and 444 km radius from the center of circulation and at the two freezing levels. The number in the parentheses are the number of ESMR-5 observations. It can be seen that the mean Western Pacific typhoon has more than twice as much LHR than the mean Eastern Pacific hurricane.

The fraction of LHR contained within the inner 222 km is calculated for a "mean" mature storm by simply computing the radio of the 222 km LHR and the 444 km LHR in the table. The results are shown in the third line. The hurricanes of the Eastern Pacific are obviously, in the mean, more compact than their Western Pacific counterparts. The last line demonstrates that there is a smaller contribution from heavier rain rates (>5 mmh^{-1}) to the total rainfall for Eastern Pacific hurricanes.

TABLE 3

MEAN ESMR-5 DERIVED RAINFALL PARAMETERS OF WESTERN PACIFIC TYPHOONS AND EASTERN PACIFIC HURRICANES

	5.0 km FREEZING LEVEL		4.5 km FREEZING LEVEL
	W. PACIFIC TYPHOONS (12)	E. PACIFIC HURRICANES (11)	E. PACIFIC HURRICANES (11)
LHR (222 km)	4.4×10^{14}W	1.6×10^{14}W	2.2×10^{14}W
LHR (444 km)	8.7×10^{14}W	2.1×10^{14}W	3.6×10^{14}W
FRACTION OF THE LHR WITHIN 222 km	.51	.76	.61
PRECIPITATION INTENSITY PARAMETER (PIP)	.36	.27	.26

Thus, the results of this comparison, although not conclusive because of the small number of ESMR-5 observations, indicate that the Eastern Pacific hurriance have less LHR, are more compact and have less intense rainfall rates. Sadler (1964) observed from TIROS images that Eastern Pacific tropical cyclone are smaller than those of the Western Pacific. He attributed the difference in size to the relatively close proximity of cold water north and south of the area where the tropical cyclones occur. Most of the tropical cyclones move out of the limited area of warm water into regions of colder water where there is less latent and sensible heat available for storm development.

5. CONCLUSIONS

Data from the Electrically Scanning Microwave Radiometer on Nimbus 5 (ESMR-5) have been used to calculate total tropical cyclone Latent Heat Release (LHR) and rainfall parameters for over 70 satellite observation of 21 tropical cyclones during 1973, 1974, and 1975 in the North Pacific tropical ocean. The data have been shown to be useful in determining the rainfall characteristics of these storms and appear to be potentially useful in monitoring and short term prediction of their intensity.

Comparison of the ESMR-5 derived total storm rainfall calculations with previous estimates based on moisture budget computation or composited rainfall statistics indicate good agreement for both mature systems (typhoons) and disturbances, except in the inner core where ESMR-5 measurements seem to underestimate rainfall rate. The calculations confirm that total typhoon rainfall is approximately twice that found in disturbances.

Case studies as well as composite studies indicate that the increase in the ESMR-5 derived LHR corresponds to storm intensification. In addition, the relative contribution of the heavier rainfall rates to the total storm rainfall also increases as was evident in the PIP calculations. There is also a tendency for the rainfall to concentrate towards the center during intensification. It also appears that these ESMR-5 derived rainfall parameters can be used to detect the beginning of tropical cyclone intensification. By monitoring the trend of increasing LHR, the first indication of tropical cyclone intensification may be obtained 1 to 2 days prior to the tropical cyclone being named and often prior to the first reconnaissance aircraft observation. Further, the time of maximum intensity may be estimated by observing the time of maximum LHR. There appears to be a 1-2 day lag relationship between maximum LHR and maximum tropical cyclone intensity.

In addition, the comparison of the Eastern Pacific ocean hurricanes and Western Pacific ocean typhoon shows that the Eastern Pacific storms have less LHR, are more compact, and have less intense rainfall.

References

Adler, R. F. and E. B. Rodgers, 1977: Satellite-observed latent heat release in a tropical cyclone. Mon. Wea. Rev., 105, 956-963.

Allison, L. J., E. B. Rodgers, T. T. Wilheit, and R. W. Felt, 1974: Tropical cyclone rainfall as measured by Nimbus 5 electrically scanning microwave radiometer, Bull. Amer. Meteor. Soc., 55 1074-1089.

Anthes, R. A., 1972: Development of asymmetries in a three-dimensional numerical model of the tropical cyclone. Mon. Wea. Rev., 100, 461-476.

Arnold, C. P., 1977: Tropical Cyclone Cloud and Intensity Relationships. Atmos. Sc. Paper. No. 277, Colorado State University, 154 pp.

Bell, G. J. and Tsui Kar-Sing, 1973: Some Typhoon Soundings and their comparison with Sounding in hurricanes. J. Appl. Meteor., 12, 74-93.

Churney, J. G., and A. Eliassen, 1964: On the growth of the hurricane depression. J. Atmos. Sci., 21, 68-75.

Dvorak, V. R., 1975: Tropical cyclone intensity analysis and forecasting from satellite imagery. Mon. Wea. Rev., 103, 420-430.

Erickson, S. L. 1977: Comparison of Developing vs Non-Developing Tropical Disturbances. Atmos. Sc. Paper No. 274, Colorado State University, 81 pp.

Frank, W. M., 1977: The structure and energetics of the tropical cyclone. Part 1: Storm structure. Mon. Wea. Rev., 105, 1119-1135.

Gray, W. M., E. Ruprecht, and R. Phelps, 1975: Relative humidity in tropical weather systems. Mon. Wea Rev., 103, 8, 685-690.

Gentry, R. C., E. Rodgers, J. Steranka, and W. Shenk , 1980: Predicting tropical cyclone intensity using satellite measured equivalent blackbody temperatures of cloud tops. To be published in Mon. Wea Rev.

Hawkins, H. F. and D. Rubsam, 1968: Hurricane Hilda, 1964: Part II. Mon Wea. Rev., 96, 617-636

Hughes, L. A., 1952: On the low-level wind structure of tropical storms. J. Meteor., 9, 422-428.

Jordan, E. A., 1958: Mean Sounding for the West Indies areas. J. Appl. Meteor., 15, 91-97.

Kurihara, Y., 1975: Budget analysis of a tropical cyclone simulated in an axisymmetric numerical model. J. Atmos. Sci., 32, 25-59.

Lovejoy, S. and G. L. Austin, 1979: The estimation of rain from satellite borne microwave radiometers. Submitted Quart J. R. Met Soc.

References (Continued)

Miller, B. E., 1958: Rainfall rates in Florida hurricanes. Mon. Wea. Rev., 86, 258-264.

_____, 1962: On the momentum and energy balance of hurricane Helene (1958). Report No. 53, National Hurricane Research Project, 19 pp.

Nordberg, W., J. Conaway, D. B. Ross and T. T. Wilheit, 1971: Measurement of microwave emissions from a foam-covered wind driven sea. J. Atmos. Sci., 28, 429-435.

Ooyama, K., 1964: A dynamical model for the study of tropical cyclone development. Geoffis Intern., 4, 187-198.

Palmen, E. and C. W. Newton, 1969: Atmospheric Circulation System. Academic Press, 381-383 and 481.

_____, and H. Riehl, 1957: Budget of angular momentum and energy in tropical cyclones. J. Meteor., 14, 150-159.

Riehl, H. and J. Malkus, 1961: Some aspects of Hurricane Daisy, 1958. Tellus, 13, 181-213.

Robinson, M. K. and R. A. Baurer, 1971: Atlas of monthly mean sea surface and subsurface temperature and depth of the top of the thermocline North Pacific ocean. NEPRF TP 7-76, Monterey, Calif. 24 pp.

Rosenthal, L., 1978: Numerical simulation of tropical cyclone development with latent heat release by the resolvable scales, I: Model description and preliminary results, J. of Atmos. Sci., 35, 258-271.

Sadler, J. 1964: Tropical cyclones of the eastern North Pacific as revealed by TIROS observations. J. Appl. Meteor., 3, 347-366.

Tuleya, R. E., and Y. Kurihama, 1975: The energy and angular momentum budget of a three-dimensional tropical cyclone mode. J. Atmos. Sci., 32, 287-301.

U. S. Fleet Weather Center/Joint Typhoon Warning Center, 1973: Annual Typhoon Report, U. S. Navy Report, Guam, 94 pp.

U. S. Fleet Weather Center/Joint Typhoon Warning Center, 1974: Annual Typhoon Report, U. S. Navy Report, Guam, 113 pp.

U. S. Fleet Weather Center/Joint Typhoon Warning Center, 1975: Annual Typhoon Report, U. S. Navy Report, Guam, 75 pp.

Wilheit, T. T., 1972: The electrically scanning microwave radiometer (ESMR) experiment. Nimbus 5 Users Guide, NASA Goddard Space Flight Center, 55-105.

_____, T. C. Chang, M. S. V. Rao, E. B. Rodgers and J. S. Theon, 1977: A satellite technique for quantitatively mapping rainfall rates over the oceans. J. Appl. Meteor., 16, 551-560.

Williams, K. T., and Gray, W. M., 1973: A statistical analysis of satellite-observed trade wind cloud clusters in the Western North Pacific, Tellos, 21, 323-336.

Zehr, R., 1976: Tropical disturbances intensification. Atmos. Sc. Paper. No. 259, Colorado State University, 19 pp.